



**HAL**  
open science

## Direct incorporating small amount of Ce (III) in Cu-SAPO-18 catalysts for enhanced low-temperature NH<sub>3</sub>-SCR activity: Influence on Cu distribution and Si coordination

Qin Wu, Chi Fan, Ya Wang, Xiaoping Chen, Guimin Wang, Zhengxing Qin, Svetlana Mintova, Junhua Li, Jianjun Chen

### ► To cite this version:

Qin Wu, Chi Fan, Ya Wang, Xiaoping Chen, Guimin Wang, et al.. Direct incorporating small amount of Ce (III) in Cu-SAPO-18 catalysts for enhanced low-temperature NH<sub>3</sub>-SCR activity: Influence on Cu distribution and Si coordination. *Chemical Engineering Journal*, 2022, 435, Part 1, pp.134890. 10.1016/j.cej.2022.134890 . hal-04295894

**HAL Id: hal-04295894**

**<https://hal.science/hal-04295894v1>**

Submitted on 20 Nov 2023

**HAL** is a multi-disciplinary open access archive for the deposit and dissemination of scientific research documents, whether they are published or not. The documents may come from teaching and research institutions in France or abroad, or from public or private research centers.

L'archive ouverte pluridisciplinaire **HAL**, est destinée au dépôt et à la diffusion de documents scientifiques de niveau recherche, publiés ou non, émanant des établissements d'enseignement et de recherche français ou étrangers, des laboratoires publics ou privés.

**Direct incorporating small amount of Ce (III) in Cu-SAPO-18 catalysts for enhanced low-temperature NH<sub>3</sub>-SCR activity: influence on Cu distribution and Si coordination**

Qin Wu<sup>a,b,‡</sup>, Chi Fan<sup>a,‡</sup>, Jianjun Chen<sup>a,\*</sup>, Ya Wang<sup>a</sup>, Xiaoping Chen<sup>a</sup>, Guimin Wang<sup>a</sup>,

Zhengxing Qin<sup>c</sup>, Svetlana Mintova<sup>c,d</sup>, Junhua Li<sup>a</sup>

<sup>a</sup> *State Key Joint Laboratory of Environment Simulation and Pollution Control,*

*School of Environment, Tsinghua University, Beijing, 100084, China.*

<sup>b</sup> *Key Laboratory of Material Chemistry for Energy Conversion and Storage, Ministry*

*of Education, School of Chemistry and Chemical Engineering, Huazhong University*

*of Science and Technology, Wuhan, 430074, China.*

<sup>c</sup> *State Key Laboratory of Heavy Oil Processing, College of Chemical Engineering,*

*China University of Petroleum (East China), Qingdao, 266580, China.*

<sup>d</sup> *Normandie Univ, ENSICAEN, UNICAEN, CNRS, Laboratoire Catalyse et*

*Spectrochimie, 6 Boulevard Maréchal Juin, 14050 Caen, France.*

\*Corresponding author: [chenjianjun@tsinghua.edu.cn](mailto:chenjianjun@tsinghua.edu.cn)

‡ These authors contributed equally.

**Abstract:** The reduction of NO<sub>x</sub> emission during the cold start period of diesel vehicles requires special attention in accordance with the emission regulations. In this work, the direct incorporation of cerium and copper in SAPO-18 catalyst with AEI type framework structure (CuCe-SAPO-18) resulting in a substantial enhancement of the performance in the low-temperature NH<sub>3</sub>-SCR reaction (<200 °C). A small amount of cerium (0.13–0.31 wt.%) broadened the reaction temperature range of use and increased the hydrothermal stability of the catalyst considerably. The cerium species was introduced in the ion-exchange sites of Cu-SAPO-18 in the form of Ce<sup>3+</sup> ions even with high loading (3.15 wt.%). The Ce<sup>3+</sup> ions were found to affect the distribution of silicon and aluminum atom coordination (<sup>29</sup>Si-NMR, <sup>27</sup>Al MAS NMR) in the AEI-type skeleton structure leading to an increase of both the amount of active Cu<sup>2+</sup> species and the acidity of the CuCe-SAPO-18 catalysts that are beneficial for the NH<sub>3</sub>-SCR reaction.

**Keywords:** CuCe-SAPO-18; One-pot synthesis; Low-temperature activity; Active Cu<sup>2+</sup> ions; Acidity

## 1. Introduction

Nitrogen oxides (NO<sub>x</sub>) originated from diesel tail gas are one of the main air pollutants and environmental concerns [1–3]. In recent decades, selective catalytic reduction with ammonia (NH<sub>3</sub>-SCR) technology utilizing SCR catalyst to reduce NO<sub>x</sub> to N<sub>2</sub> and H<sub>2</sub>O by NH<sub>3</sub> is successfully commercialized and widely used [4–6]. More restricted demands for NO<sub>x</sub> emission are issued worldwide including the ultra-low NO<sub>x</sub> emissions raised by the California Air Resource Board (CARB) and the increased

weighting factor at low rotate speed/load for novel WHTC/WHSC cycle tests in China NS VI. The reduction of NO<sub>x</sub> from diesel vehicles during the cold start period (exhaust temperature below 200 °C) becomes an important and urgent task [7–9].

At present, small pore Cu-based zeolites including CHA-type structure (Cu-SSZ-13 and Cu-SAPO-34) and AEI-type structure (Cu-SSZ-39 and Cu-SAPO-18) are selected as SCR catalysts owing to their high catalytic activity and sufficient hydrothermal stability [10,11]. The Cu-AEI catalyst was reported to be highly active and more robust than Cu-CHA [12,13]. The Cu-AEI catalyst and more specifically the silicoaluminophosphate (Cu-SAPO-18) can be synthesized with high solid yields and various Si/Al ratio in comparison to the Cu-CHA (Cu-SSZ-39) using a common organic template [14].

To further enhance the performance of the SCR catalyst, the addition or doping with a second metal (promoter) is believed to be effective [15–17]. According to the previous research, the second metal would have the following effects: (1) Increasing the number of active sites. The Cu<sup>2+</sup> species are generally accepted as the main active sites for SCR reaction so that many efforts have been made to provide higher amount of Cu<sup>2+</sup> species [18–21]. Chen et al. [19] proposed a strategy to result in an effective migration of indigenous Cu<sup>2+</sup> ions in 8MR to D6R sites of Cu-SSZ-13 which are more active at low temperature by introducing larger ions such as Ce<sup>4+</sup> and La<sup>3+</sup>. The cerium and lanthanum with tetraethylenepentamine (TEPA) formed a Ce/La-TEPA complex occupying the exchange-sites of the SSZ-13. (2) Inhibiting metal oxides aggregations. The oxidation of Cu species and the consequent aggregation of the CuO<sub>x</sub> are considered

as a primary reason for the hydrothermal deactivation of Cu-based zeolite catalyst. Therefore, the stabilization of Cu species during the hydrothermal treatment is vital [22–26]. Usui et al. [23] tried to improve the hydrothermal stability of aluminum-rich Cu-SSZ-13 by loading cerium. A small loading of cerium (0.2–0.4 wt.%) was found to be sufficient and ensure stabilization of the catalyst. Based on Rietveld refinement of XRD patterns, it was found that the appropriate number of cerium may occupy the ion-exchange sites of Cu-SSZ-13 and stabilize the  $\text{Cu}^{2+}$  ions during the hydrothermal treatment. (3) Suppressing the formation and deposition of poison species over the catalyst. A core-shell structure with a protective layer on the external surface of a catalyst, could efficiently prevent the detrimental effect of  $\text{SO}_2$  and  $\text{H}_2\text{O}$  via adsorption and thus to improve the stability of the catalyst [27–29]. Li et al. [29] deposited a  $\text{CeO}_2$  film on the surface of Cu-SAPO-18, and the thickness of the film was carefully tuned. This advanced core-shell catalyst showed a satisfactory NO conversion and resistance towards steam and  $\text{SO}_2$ .

Yet, using metal promoter is already known but to the best of our knowledge, few reports on the improvement of the low-temperature activity of Cu-SAPO-18 catalysts are available. Hence, the introduction of an appropriate metal promoter to optimize the performance of Cu-SAPO-18 catalyst in the  $\text{NH}_3$ -SCR reaction is the goal of this investigation. The effect of cerium addition towards improving the low-temperature performance of Cu-SAPO-18 in the  $\text{NH}_3$ -SCR reaction is studied in details. The method for cerium addition is investigated too. The traditional method includes an ion-exchange using either parent zeolite support or as-prepared Cu-based catalyst with a

cerium precursor solution. However, due to the low ion-exchange capacity and the small opening pore of AEI type material, a low amount of cerium can be introduced. Most of these metal species are deposited on the surface leading to a poor reproducibility. More importantly, some of the silicoaluminophosphates are not stable during the ion-exchange process [30,31].

Herein, we report on the modification of Cu-SAPO-18 by cerium using a direct one-pot method. Utilizing tetraethylenepentamine (TEPA) and N, N-diisopropylethylamine (DIPEA) as dual-templates allowed the introduction of cerium with a loading of 0–3.15 wt.% in the CuCe-SAPO-18 catalyst. Loading a small quantity of cerium (0.13–0.31 wt.%) is found sufficient to ensure both excellent activity and hydrothermal stability of the catalyst in the NH<sub>3</sub>-SCR reaction. The effect of cerium on the physicochemical properties of CuCe-SAPO-18 catalyst is evaluated by XRD, EPR, in situ DRIFT, <sup>29</sup>Si-NMR and NH<sub>3</sub>-TPD characterizations. Furthermore, the state of cerium in the catalyst is characterized experimentally and by DFT modeling.

## 2. Experimental

### 2.1. Synthesis

CuCe-SAPO-18 catalysts were prepared using a one-pot synthesis by hydrothermal method. The catalysts with different cerium contents were prepared from precursor mixtures with the following molar ratio: 1.0 Al<sub>2</sub>O<sub>3</sub>: 0.90 P<sub>2</sub>O<sub>5</sub>: 1.20 SiO<sub>2</sub>: 1.55 DIPEA: 0.1 Cu: 0.2 TEPA: m CeO<sub>2</sub>: 45 H<sub>2</sub>O, where m=0.002, 0.006, 0.01, 0.04, 0.08. Tetraethylenepentamine (TEPA, 95%, Aladdin) and N, N-diisopropylethylamine (DIPEA, 99%, Sigma-Aldrich) as templates were used. In a typical synthesis procedure,

Cu-TEPA complex was first formed by stirring CuSO<sub>4</sub> aqueous solution and TEPA for 0.5 h. Second, a certain amount of cerous nitrate was dissolved into the above solution and continually stirred for 0.5 h. Third, H<sub>3</sub>PO<sub>4</sub> (85 wt.%, Aladdin) silicon solution (40 wt.% SiO<sub>2</sub>, Sigma-Aldrich), pseudo boehmite and DIPEA were dropped into the mixture. The final gel was transferred into an autoclave with a Teflon liner and heated at 180 °C for 96 h. The product was purified and dried at 100 °C for 12 h and calcined at 600 °C for 5 h. The samples synthesized with different cerium contents were named as CuCe-SAPO-x, where x stands for the cerium weight content determined by ICP results. The cerium-free sample was named as Cu-SAPO-18.

## **2.2. Experimental test**

A variety of techniques were used to analyze the structural characteristics, redox and acidity of the catalyst. The performance of the samples in the NH<sub>3</sub>-SCR reaction was evaluated in a fixed-bed reactor; the measurements with a powder sample (40–60 mesh) loaded in a quartz tube were performed. The related details can be found in the Supporting Information.

## **2.3. The reaction kinetics experiment**

The experiments performed to follow the reaction kinetics were carried out to investigate the contribution of cerium to the NO reduction over the catalysts with different cerium contents at low temperatures. The NH<sub>3</sub> and O<sub>2</sub> gaseous concentration was kept at 500 ppm and 5%, respectively, while the NO concentration varied from 300 to 700 ppm. A high GHSV (i.e. 370 000–1 550 000 mL/(g·h)) was selected to obtain a low NO conversion (<20%) in order to eliminate the effect caused by the inner and

external diffusion. According to previous studies [32–34], the NH<sub>3</sub>-SCR reaction rate (i.e.,  $\delta_{\text{SCR}}$ ) of catalysts was described as:  $\delta_{\text{SCR}} = k_{\text{L-H}} + k_{\text{E-R}}[\text{NO}(\text{g})]$ , where  $\delta_{\text{SCR}}$  and  $[\text{NO}(\text{g})]$  represents the N<sub>2</sub> formation rate and gaseous NO concentration (ppm), respectively.  $k_{\text{L-H}}$  and  $k_{\text{E-R}}$  represent the kinetic reaction constant through the Langmuir-Hinshelwood (L-H) mechanism and the Eley-Rideal (E-R) mechanism, respectively. Therefore,  $k_{\text{L-H}}$  and  $k_{\text{E-R}}$  were obtained through the linear regression of the N<sub>2</sub> formation rates and NO concentration; the  $k_{\text{L-H}}$  is calculated from the intercept and  $k_{\text{E-R}}$  is derived from the slope of this regression.

## 2.4. Computational method

The Vienna Ab Initio Package (VASP) was used for the density functional theory (DFT) calculations within the generalized gradient approximation (GGA) using the PBE formulation [35–37]. The projected augmented wave (PAW) potentials were chosen to describe the ionic cores and take valence electrons into account using a plane wave basis set with a kinetic energy cutoff of 400 eV [38,39]. Partial occupancies of the Kohn-Sham orbitals were allowed using the Gaussian smearing method and a width of 0.05 eV. The electronic energy was considered self-consistent when the energy change was smaller than 10<sup>-5</sup> eV. A geometry optimization was considered convergent when the force change was smaller than 0.02 eV/Å.

The equilibrium lattice constants of orthogonal AlPO-18 unit cell were optimized, when using the  $\Gamma$  point in the Brillouin zone for Brillouin zone sampling:  $a = 13.656 \text{ \AA}$ ,  $b = 11.742 \text{ \AA}$  and  $c = 17.633 \text{ \AA}$ . The AlPO-18 unit cell model containing 24 Al, 24 P, and 96 O atoms was used for the calculations. During structural optimizations, the  $\Gamma$  point

in the Brillouin zone was used for k-point sampling, and all atoms were allowed to relax. Various locating positions for both Cu and Ce atoms were tested.

In order to compare the valence state of Ce atoms in the AlPO-18 with that in  $\text{Ce}_2\text{O}_3$  and  $\text{CeO}_2$ , unit cells of  $\text{Ce}_2\text{O}_3$  and  $\text{CeO}_2$  were calculated as well. For these calculations, the on-site corrections (DFT+U) have been applied to the 3d electron of Ce atoms ( $U_{\text{eff}}=4.5$  eV) [40]. The equilibrium lattice constants of hexagonal  $\text{Ce}_2\text{O}_3$  unit cell were optimized using a  $13 \times 13 \times 7$  k-point grid in the Brillouin zone for Brillouin zone sampling:  $a=b=3.791$  Å and  $c=6.181$  Å. The equilibrium lattice constant of cubic fluorite-type  $\text{CeO}_2$  unit cell was optimized, when using a  $11 \times 11 \times 11$  k-point grid in the Brillouin zone for Brillouin zone sampling:  $a=5.500$  Å. The atomic charges were obtained from Bader's analysis based on the numerical implementation [41].

### 3. Results and discussion

#### 3.1. Physicochemical properties of CuCe-SAPO-x catalysts

**Table 1.** Physicochemical properties of as-synthesized samples.

Sample	Cu <sup>a</sup> (wt. %)	Ce <sup>a</sup> (wt. %)	Si/(Si+Al+P) <sup>b</sup>	Al/(Si+Al+P) <sup>b</sup>	$S_{\text{BET}}^c$ (m <sup>2</sup> /g)	$V_t^d$ (cm <sup>3</sup> /g)
Cu-SAPO-18	1.87	0	0.254	0.396	372	0.178
CuCe-SAPO-0.13	1.84	0.13	0.253	0.408	407	0.198
CuCe-SAPO-0.31	1.81	0.31	0.256	0.407	413	0.199
CuCe-SAPO-0.50	1.81	0.50	0.256	0.413	363	0.170
CuCe-SAPO-1.52	1.84	1.52	0.264	0.400	366	0.177
CuCe-SAPO-3.15	1.81	3.15	0.266	0.396	367	0.179

<sup>a</sup> Determined by the ICP-OES measurement. <sup>b</sup> Determined by the XRF measurement.

<sup>c</sup> Calculated by the BET method. <sup>d</sup> Calculated by the t-plot method.

The chemical composition of the as-synthesized samples is summarized in [Table 1](#). The samples have similar content of Si, Al, P, and Cu ( $\text{Si}/(\text{Si}+\text{Al}+\text{P})=0.25$  and  $\text{Al}/(\text{Si}+\text{Al}+\text{P})=0.40$  and the Cu loading is about 1.80 wt.%), indicating that the cerium addition does not affect the chemical composition of the materials. While the cerium amount in CuCe-SAPO-x samples is varied from 0.13 % to 3.15 wt.% depending on the chemical composition of the initial gel.

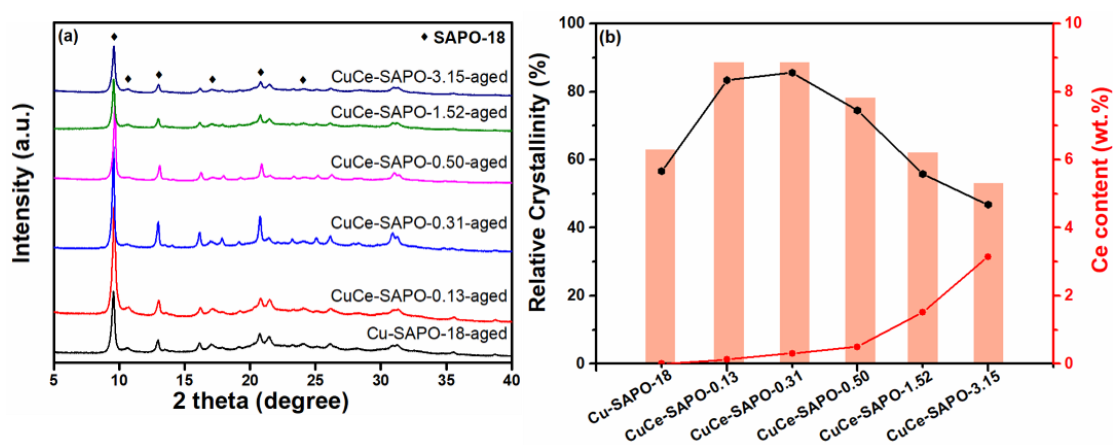


**Fig. 1.** XRD patterns of (a) the hydrothermally treated catalysts. (b) Relative crystallinity and Ce content of the hydrothermally treated catalysts.

The phase purity of the samples was examined by XRD. As shown in [Fig. S1a](#), all as-prepared samples exhibit the characteristic peaks of AEI type framework structure, indicating the successful preparation of CuCe-SAPO-18 catalysts by one-pot synthesis method [18,42]. In the samples with increased cerium content, even as CuCe-SAPO-3.15, no  $\text{CeO}_2$  diffraction peaks are present in the XRD pattern ([Fig. S1b](#)). The impact of cerium loading on the hydrothermal stability of Cu-SAPO-18 was also evaluated by XRD ([Fig. 1a](#)). After hydrothermal treatment at 750 °C for 16 h, although the catalyst maintains the AEI type framework structure, the peaks intensity is lower than for the as synthesized catalyst. The relative crystallinity of the aged samples compared to the

fresh ones is shown in Fig. 1b. A significant difference is observed after sample CuCe-SAPO-0.31, the degradation of crystallinity is evident (Fig. 1b). These results suggest that the hydrothermal stability of the Cu-SAPO-18 is enhanced only after addition of a small amount of cerium (0.13 and 0.31 wt.%), i.e., samples CuCe-SAPO-0.13 and CuCe-SAPO-0.31 almost preserved their crystallinity.

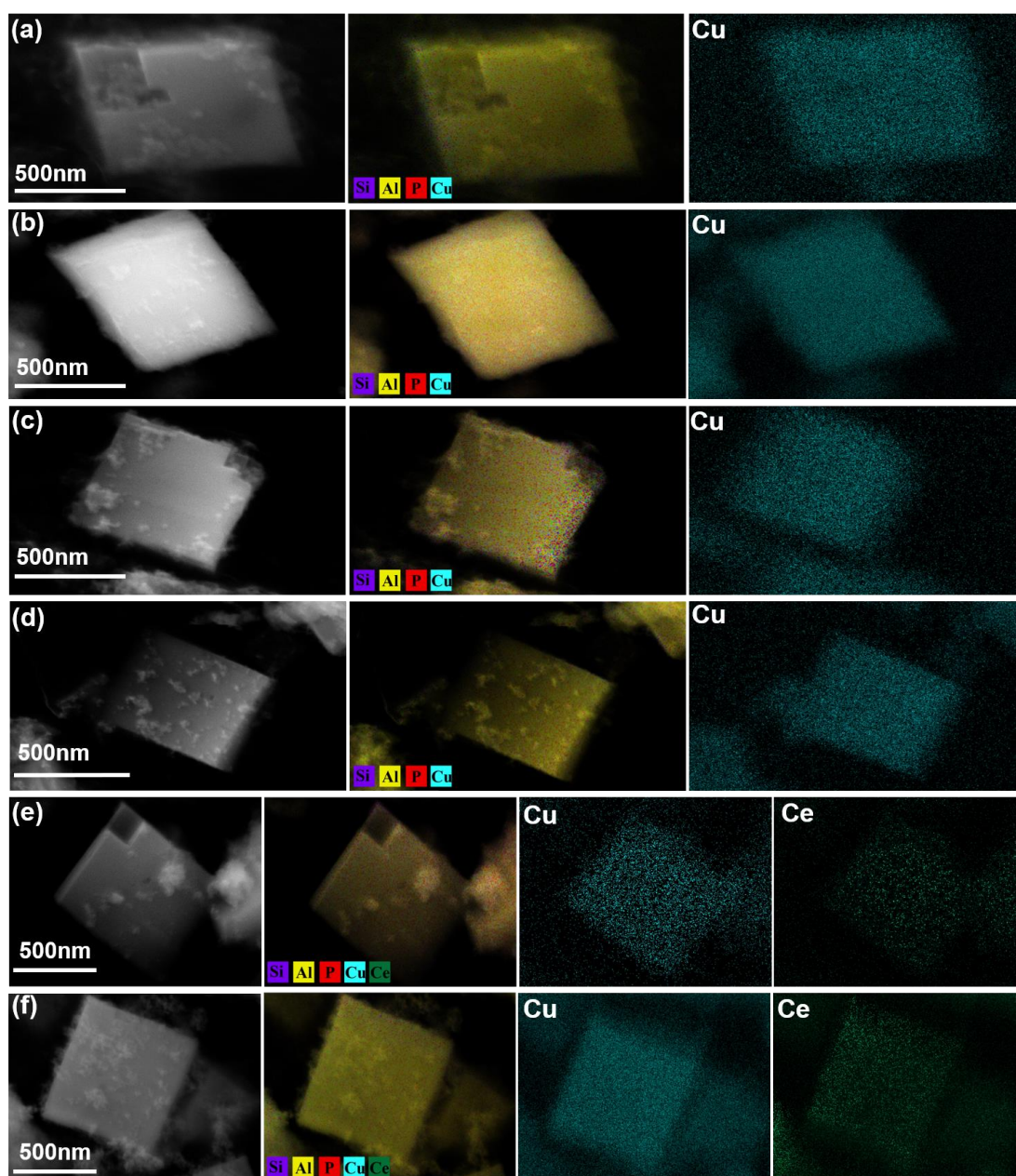


**Fig. 2.** SEM-EDS mappings of (a) Cu-SAPO-18, (b) CuCe-SAPO-0.13, (c) CuCe-SAPO-0.31, (d) CuCe-SAPO-0.50, (e) CuCe-SAPO-1.52, and (f) CuCe-SAPO-3.15

samples.

The dispersion of cerium species in the catalysts was examined by SEM-EDS element mapping (Fig. 2, Fig. S2). Due to the low cerium content in samples CuCe-SAPO-0.13, -0.31, and -0.50, the precision of the EDS measurements was low. The cerium mapping for samples CuCe-SAPO-1.52 and -3.15 are shown in Fig. 2e-f. The high homogeneity of the samples (Si, Al, and P) confirmed that the one-pot synthesis is an appropriate synthesis method. The high concentration of cerium does not lead to formation of Ce clusters suggesting that the cerium species are uniformly distributed. This result is consistent with the XRD data shown above.

### 3.2. Performance of CuCe-SAPO-x catalysts in NH<sub>3</sub>-SCR reaction

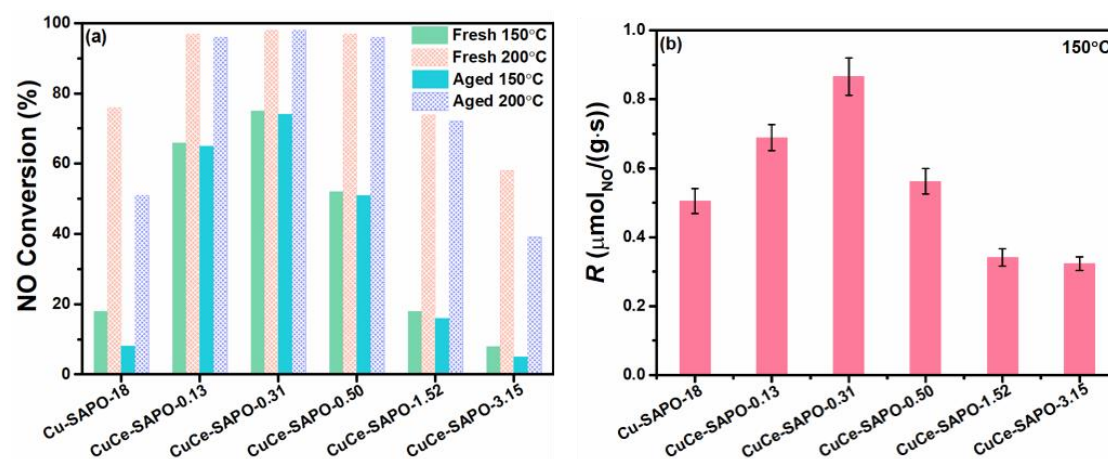


**Fig. 3.** NH<sub>3</sub>-SCR performance of (a) fresh and hydrothermally aged catalysts at 150 °C and 200 °C, and (b) reaction rates over the fresh catalysts at 150 °C.

The performances of the catalysts before and after hydrothermal treatment in the NH<sub>3</sub>-SCR reaction was evaluated. The focus was on the NO conversion at low temperatures (150 °C and 200 °C). As shown in Fig. 3a, the cerium-free sample, Cu-SAPO-18, shows a NO conversion of 18% and 76% at 150 °C and 200 °C, respectively. In comparison, the NO conversion at 150 °C increases evidently to 65% and 75% when

the cerium loading in the Cu-SAPO-18 sample increases slightly from 0 to 0.13 and 0.31 wt.% (samples CuCe-SAPO-0.13 and CuCe-SAPO-0.31), respectively. The NO conversion on these cerium-loaded samples increases further to approximately 98% at 200 °C. A continuous increase of the cerium loading on samples CuCe-SAPO-0.50, CuCe-SAPO-1.52, and CuCe-SAPO-3.15 causes, however, a gradual decrease in NO conversion activity. In the case of sample CuCe-SAPO-3.15, the NO conversion rate is even lower than that of Cu-SAPO-18 in the whole temperature range studied (Fig. S3a), pointing to the negative impact of high cerium loading on the NO reduction. Apparently, an appropriate amount of cerium can improve substantially the NH<sub>3</sub>-SCR activity and specially the catalytic conversion of NO at low temperature. The reaction rates calculated from kinetics experiment at 150 °C also demonstrate the activity improvement (Fig. 3b). The CuCe-SAPO-0.31 catalyst resulted in an about 1.7-fold increase in the NH<sub>3</sub>-SCR reaction rate at 150 °C compared to that of the Cu-SAPO-18 catalyst (Fig. 3b). In addition, the active temperature window for the catalysts loaded with cerium is also expanded (Fig. S3a). The temperature range of NO conversion >90% (T<sub>90</sub>) for Cu-SAPO-18 is 225–400 °C, while that for the CuCe-SAPO-0.31 is expanded to 200–500 °C. The hydrothermal aging causes a loss in NO conversion rate especially in the high temperature range >350 °C (Fig. S3b). This is due to the structure degradation of SAPO-18 which was evidenced by XRD (see Fig. 1). As expected, both CuCe-SAPO-0.13 and CuCe-SAPO-0.31 catalysts show high NO conversion rate within the temperature range studied, and the low-temperature deNO<sub>x</sub> activity almost maintains (Fig. 3a), highlighting the outstanding hydrothermal stability of CuCe-

SAPO-x catalysts modified with an appropriate amount of cerium. In addition, we have tested the stability of Cu-SAPO-18 and CuCe-SAPO-0.31 during long-term NH<sub>3</sub>-SCR under the investigated conditions at 200 °C (Fig. S4). Obviously, the NO conversion on the catalysts remained basically unchanged in a span of 24 h, indicating that the CuCe-SAPO-x catalysts could remain stable over a long-term NH<sub>3</sub>-SCR test.

The N<sub>2</sub>O yield is considered as an important aspect of NH<sub>3</sub>-SCR catalyst. As shown in Fig. S3a, the N<sub>2</sub>O yields is lower than 10 ppm for all as-synthesized catalysts over the entire temperature range. While after the hydrothermal treatment, the aged catalysts yield more N<sub>2</sub>O than the fresh counterparts (Fig. S3b). Yet still the CuCe-SAPO-0.13-aged and CuCe-SAPO-0.31-aged show the lowest N<sub>2</sub>O yields (<10 ppm) among the samples thus proving the great effect of cerium in an appropriate concentration on catalysts stability.

### 3.3. Effect mechanism of Ce addition on low-temperature NH<sub>3</sub>-SCR of catalysts

#### 3.3.1. The existence of Ce species in the catalysts

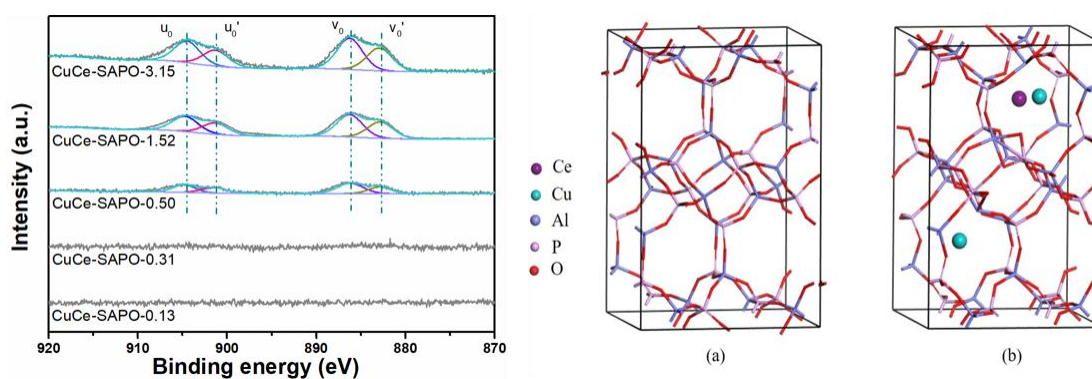


**Fig. 4.** Ce 3d XPS spectra of as-synthesized CuCe-SAPO-x catalysts (left) and DFT optimized structures of (a) pure AlPO-18 and (b) Cu and Ce loaded CuCe-SAPO-x catalysts (right).

To study the chemical states of cerium, XPS analysis of the samples was performed. The Ce 3d spectra of CuCe-SAPO-x catalysts are shown in Fig. 4, and no

peaks due to cerium species are observed in CuCe-SAPO-0.13 and CuCe-SAPO-0.31 samples. The XPS technique is a surface sensitive analytical method with a limited detection depth in the range of 1–10 nm [43,44]. Therefore, we could conclude that in samples CuCe-SAPO-0.13 and CuCe-SAPO-0.31, the cerium species are either highly dispersed on the surface of catalyst which is below the detection limit or are located in the internal structure of zeolite. With increasing the cerium content in samples CuCe-SAPO-0.50, -1.51 and -3.52, four peaks at 886.1, 882.8, 904.5 and 901.2 eV assigned to  $Ce^{3+}$  are detected [21]. It was suggested that  $Ce^{3+}$  ions are major cerium species located on the surface of a catalyst even after a high amount of cerium added [20,21,45]. Interestingly, in our present study, even in sample CuCe-SAPO-3.15 with the highest cerium content, the  $Ce^{4+}$  ions are hardly detected by XPS. Further the valence states of cerium in samples CuCe-SAPO-x is study by DFT calculations. The optimized structures of CuCe-SAPO-x with the Cu and Ce location is shown in Fig. 4. The results demonstrate that both Cu and Ce ions preferably occupy the center of 8MR. Based on the optimized structure, the cerium atom in CuCe-SAPO-x is calculated to contain 10.32 outer electrons. When it comes to the cerium atom in  $Ce_2O_3$  and  $CeO_2$ , the number of outer electrons in each structure is 10.00 and 9.60, respectively. Compared to the neutral cerium atoms containing 12 outer electrons, the cerium atom in the CuCe-SAPO-x loses 1.68 electrons, which is more in line with the lost 2.00 electrons of that in  $Ce_2O_3$  rather than 2.40 electrons in  $CeO_2$ . As a result, it is speculated that the valence state of cerium species in CuCe-SAPO-18 is close to +3 and much smaller than +4.

**Table 2.** Rietveld refinement results of as-synthesized CuCe-SAPO-x catalysts.

Sample	Ce (wt. %)	x	y	z	Occupancy	$R_{wp}$ (%)
Cu-SAPO-18	0	-	-	-	-	0.26
CuCe-SAPO-0.13	0.13	0.78010	1.09210	0.25280	0.0233	0.28
CuCe-SAPO-0.31	0.31	0.78010	1.09210	0.25280	0.0566	0.30
CuCe-SAPO-0.50	0.50	0.78010	1.09210	0.25280	0.0911	0.34
CuCe-SAPO-1.52	1.52	0.78010	1.09210	0.25280	0.2726	0.39
CuCe-SAPO-3.15	3.15	0.78010	1.09210	0.25280	0.5727	0.31

To further verify the location of cerium species, Rietveld refinement of the XRD patterns recorded for as-prepared samples with different cerium content (0 to 3.15 wt.%) is conducted; the results from the Rietveld refinement are shown in [Fig. S5](#) and [Table S1-6](#). The occupation sites and amount of Cu and Ce are carefully determined based on the ICP-OES results. The copper is assumed to exist as  $\text{Cu}^{2+}$  species. The distributions of  $\text{Cu}^{2+}$  species in the catalysts are found less affected by the cerium addition according to the results from  $\text{NH}_3$ -DRIFTS ([Fig. 5](#)) presented hereinafter; the respective amount of Cu in D6R and 8MR are set to be 40% and 60% ([Fig. 5b](#), [Table S9](#)). The cerium is present as  $\text{Ce}^{3+}$  based on the XPS results and probably placed in the ion-exchange sites of 8MR according to the early reports [[19,23](#)]. The atomic positions, cerium occupancy and agreement factors ( $R_{wp}$ ) from the refinement analysis are summarized in [Table 2](#). A good  $R_{wp}$  is obtained for all refinements. Then, notably, the obtained cerium occupancy which reflects the content of cerium filling the ion-exchange sites increases in proportion to the detected cerium content from 0.13 to 3.15 wt.%, implying that the cerium species reside in the ion-exchange sites as isolated ions even for the cerium

loading is up to 3.15 wt.% [23]. The XPS and XRD results show that the cerium species are present as  $\text{Ce}^{3+}$  rather than  $\text{Ce}^{4+}$  or  $\text{CeO}_2$ .

To assess the role of cerium ions in the  $\text{NH}_3$ -SCR reaction, H-SAPO-18 and the one-pot synthesized Ce-SAPO-18 (details are shown in Table S7 and Fig. S7) were examined in the  $\text{NH}_3$ -SCR reaction. The NO conversion is negligible for both H-SAPO-18 and Ce-SAPO-18 samples illustrating that cerium species is inactive for  $\text{NO}_x$  conversion. In other words, the addition of a small amount of Ce affects the reactivity of  $\text{NH}_3$ -SCR by acting on the copper species or molecular sieve structure. The amount of  $\text{Cu}^{2+}$  species and acidity of Cu-based zeolite SCR catalyst are highly important since they are responsible for the low-temperature denitrification efficiency.

### 3.3.2. The effect of Ce species on Cu species

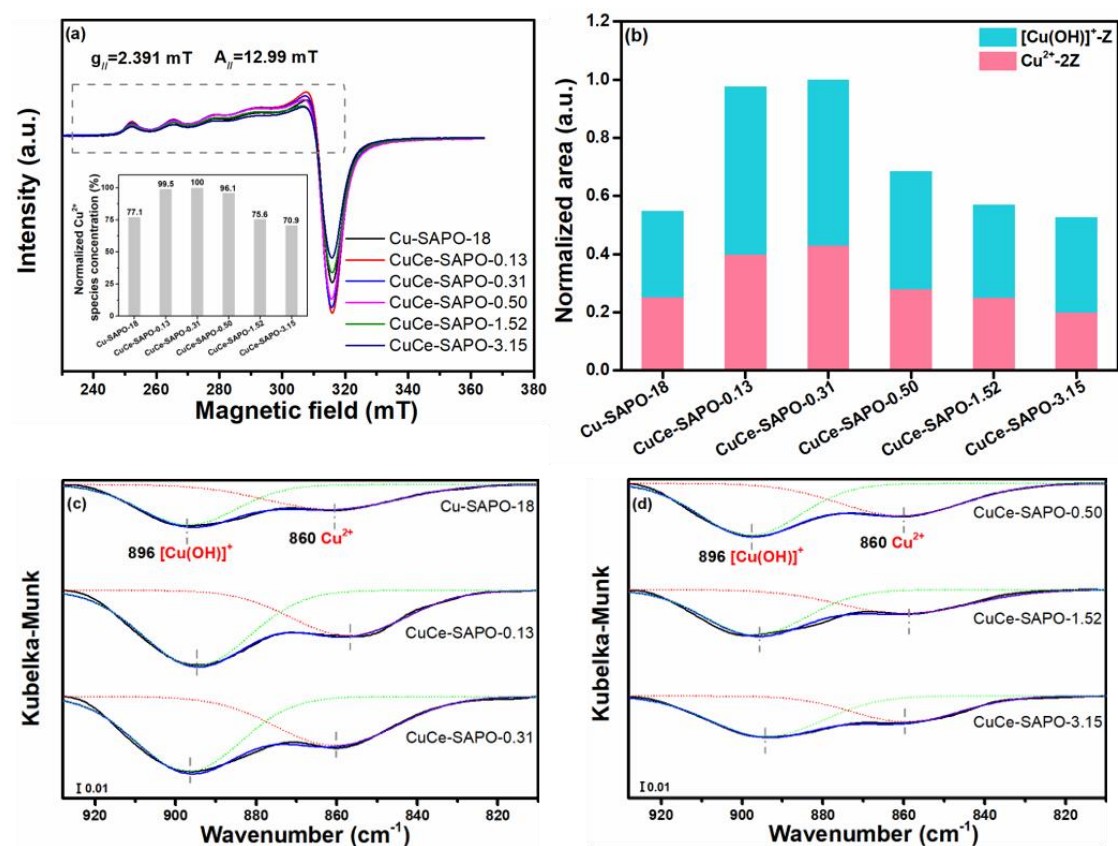


Fig. 5. (a) EPR spectra of as-synthesized catalysts, (b) amount of  $\text{Cu}^{2+}$  species

represented as normalized area from the NH<sub>3</sub>-saturated DRIFTS spectra. NH<sub>3</sub>-saturated DRIFTS spectra of (c) Cu-SAPO-18, CuCe-SAPO-0.13, CuCe-SAPO-0.31 and (d) CuCe-SAPO-0.50, CuCe-SAPO-1.52, CuCe-SAPO-3.15.

As mentioned above, the cerium addition has little effect on the total Cu loading. The probable changes in the Cu species after cerium loading were studied. The Cu<sup>2+</sup> species are the active sites in the NH<sub>3</sub>-SCR reaction and the EPR measurements toward detection of Cu<sup>2+</sup> ions are usually conducted [46–50]. Fig. 5a displays the EPR results for the freshly prepared catalysts at 93 K. Upon hydration, all samples present similar values of  $g_{\parallel} = 2.391$  and  $A = 12.99$  mT due to the presence of Cu<sup>2+</sup> species in bivalent oxidation state [51]. The quantification of total Cu<sup>2+</sup> species could be examined by double integration of the EPR spectra. The peak area of samples CuCe-SAPO-0.13 and CuCe-SAPO-0.31 is depicted as an inset in Fig. 5a, and this result indicates the abundant Cu<sup>2+</sup> species present. With further increasing the cerium content, the peak area gradually reduces and eventually is lower than the Cu-SAPO-18. The EPR result strongly suggests that the presence of a small amount of cerium loading (0.13–0.31 wt.%) favors the formation of Cu<sup>2+</sup> species which are beneficial for the NH<sub>3</sub>-SCR reaction.

According to previously reported results, two types of Cu<sup>2+</sup> ions in dehydrated Cu-CHA and Cu-AEI catalysts exist: isolated Cu<sup>2+</sup> ions in D6R balanced by a couple of framework negative charges and [Cu(OH)]<sup>+</sup> ions in 8MR balanced by only a single framework negative charge, respectively [51–55]. To probe the redistribution of Cu<sup>2+</sup> species after the introduction of cerium in the catalysts, DRIFTS experiments under NH<sub>3</sub> adsorption were conducted [51,56]. The DRIFTS spectra of NH<sub>3</sub>-adsorbed

samples are shown in Fig. 5c, d. All samples show two high-resolved negative bands centered at  $896\text{ cm}^{-1}$  and  $860\text{ cm}^{-1}$  that correspond to the  $\text{NH}_3$  adsorbed on  $[\text{Cu}(\text{OH})]^+$  and isolated  $\text{Cu}^{2+}$  ions, respectively. These bands occurred at lower wavenumbers compared to the Cu-LTA ( $962$  and  $926\text{ cm}^{-1}$ ) and Cu-CHA ( $950$  and  $900\text{ cm}^{-1}$ ), which could be explained by the different framework structure [57]. Among all, the samples CuCe-SAPO-0.13 and CuCe-SAPO-0.31 show much intense negative bands. This result is consistent with the EPR, indicating the larger number of  $\text{Cu}^{2+}$  species in these two samples. In order to elucidate the evolution of  $[\text{Cu}(\text{OH})]^+$  and isolated  $\text{Cu}^{2+}$  ions after the cerium introduction, the total area of CuCe-SAPO-0.31 is set as unity, and the areas of other samples are normalized. The proportion of two  $\text{Cu}^{2+}$  species are also calculated based on the respective peak areas and the results are presented in Fig. 5b and Table S9. Interestingly, although the total amount of  $\text{Cu}^{2+}$  species is varied, it is clear that the proportion of two  $\text{Cu}^{2+}$  species is nearly identical among the different cerium-loaded samples. The  $[\text{Cu}(\text{OH})]^+$  dominates at around 60% and the isolated  $\text{Cu}^{2+}$  ions accounts for around 40%, indicating that migration between two  $\text{Cu}^{2+}$  species is not observed. Based on the above results we could conclude that the addition of cerium may lead to a change in the amount of  $\text{Cu}^{2+}$  species but no obvious effect on the relative amount of different  $\text{Cu}^{2+}$  species is expected.

The EPR results show that the addition of cerium enhances the dispersion of  $\text{Cu}^{2+}$  species in the sample during the crystallization process. This effect is dependent on the cerium content. We demonstrated that further increase of cerium content is disadvantageous for the catalytic activity of the SAPO-18, which indicates a probable

relationship between the cerium and copper species. Xu et al. [58] reported on an interaction between Zn and Cu species in Cu/Zn-SSZ-13 by DFT, which is believed to affect the SCR performance. Unfortunately, these interactions are not fully understood. In addition, XRD refinement shows that cerium is present at the ion exchange site. It can be inferred that when a large amount of cerium is present, it will occupy the ion exchange site and reduce the amount of  $\text{Cu}^{2+}$ . In our study, the addition of cerium is found to affect the Si coordination structure resulting in different acidity. It is speculated that the number of positively charged cerium ions may affect the distribution of Si atom and Al atom.

### 3.3.3. The effect of Ce species on the coordination of Si and Al Atoms in zeolite framework

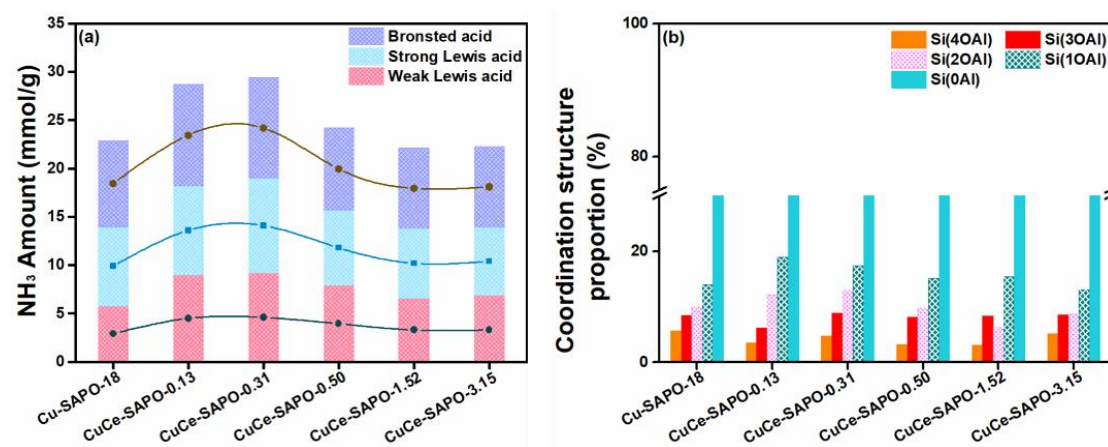


**Fig. 6.** (a)  $\text{NH}_3$  uptakes of as-synthesized catalysts with different acid sites and (b) different Si species in the as-synthesized catalysts.

The  $\text{NH}_3$ -TPD measurements for as-synthesized catalysts were conducted. As shown in Fig. S9, the peak intensity of CuCe-SAPO-x is different from the Cu-SAPO-18, indicating that the cerium affects the acidity of the catalysts. The  $\text{NH}_3$  desorption spectra of Cu-SAPO-18 and CuCe-SAPO-x catalysts are deconvoluted into three regions (Fig. S10). The low-temperature peak A (160–180 °C) is attributed to

ammonium species on weak Lewis acid sites, the medium-temperature peak B (240–270 °C) is assigned to the desorbed NH<sub>3</sub> on strong Lewis acid sites created by Cu<sup>2+</sup> ions and the high-temperature peak C (360–400 °C) belong to NH<sub>3</sub> desorption on Brønsted acid sites [18,42,59]. As displayed in Fig. 6a and Table S10, the NH<sub>3</sub> uptakes from all three acid sites are increased after addition of a small amount of cerium (CuCe-SAPO-0.13 and CuCe-SAPO-0.31). Further increase of cerium suppress the NH<sub>3</sub> adsorption on SAPO-18 remarkably (CuCe-SAPO-0.50, CuCe-SAPO-1.52, and CuCe-SAPO-3.15). A clear difference is evident by comparing the acidity of Cu-SAPO-18, CuCe-SAPO-0.31 and CuCe-SAPO-3.15. The total acidity of CuCe-SAPO-3.15 is similar to the Cu-SAPO-18, suggesting that the cerium species in the SAPO-18 have a low affinity for NH<sub>3</sub>.

To clarify the distinct changes in the acidity of the catalysts due to the presence of cerium, the Si coordination in the AEI structure was examined. <sup>29</sup>Si-NMR spectra and the peak deconvolution are shown in Fig. S11. The <sup>29</sup>Si-NMR spectra of Cu-SAPO-18 and CuCe-SAPO-x catalysts contain peaks at -89.7, -94.2, -99.4, -105.1 and -114.1 ppm attributed to Si(4OAl), Si(3OAl), Si(2OAl), Si(1OAl) and Si(0OAl), respectively [42,60]. The contribution of each peak is calculated by the Gaussian area fitting and the results are shown in Fig. 6b. The Si coordination in the AEI type structure is changed under cerium addition. The proportion of Si(0OAl), which generates Si islands by the SM3 substitution mechanism, decreases in samples CuCe-SAPO-0.13 and CuCe-SAPO-0.31 and then increases to some extent as further cerium amount increased. In addition, the ratio of Si(1OAl) and Si(2OAl) in the CuCe-SAPO-0.13 and CuCe-SAPO-

0.31 structures is much higher than for the other catalysts. It is known that the Si islands could not provide any acid sites and the acidity generated by Si coordinated in the structure increases in the following order  $\text{Si}(4\text{OAl}) < \text{Si}(3\text{OAl}) < \text{Si}(2\text{OAl}) < \text{Si}(1\text{OAl})$  [61]. The chemical composition of the samples after addition of cerium did not change, thus no conclusions for Si distribution and coordination were made [62]. The  $^{29}\text{Si}$ -NMR result (Fig. 6b, Fig. S11) implies that a small amount of cerium may influence the Si insertion mechanism during the direct one-pot hydrothermal synthesis and the SM2 substitution is more likely to occur. The formation of larger number of  $\text{Si}(1\text{OAl})$  and  $\text{Si}(2\text{OAl})$  in the CuCe-SAPO-0.13 and CuCe-SAPO-0.31 samples with high acidity is probably causing the enhanced total  $\text{NH}_3$  uptake.

The peaks in  $^{27}\text{Al}$  MAS NMR spectra (Fig. S12) around 9.1 and 53.4 ppm are assigned to octahedral and tetrahedral coordination of aluminum in catalysts, which represent extra-framework aluminum ( $\text{Al}_{\text{EF}}$ ) and framework aluminum ( $\text{Al}_{\text{TF}}$ ), respectively [63,64]. When a small amount of Ce is added, the peak intensity of the framework aluminum is significantly enhanced, indicating that Ce doping makes more aluminum into the framework. In a word, it was found through  $^{29}\text{Si}$ -NMR and  $^{27}\text{Al}$ -NMR that a small amount of Ce addition did change the coordination of silicon atoms and aluminum atoms, causing an increase in the aluminum content of the framework. With the increase of  $\text{Si}(1\text{OAl})$  and  $\text{Si}(2\text{OAl})$  contents, the Brønsted acid of zeolite skeleton is enhanced. On the other hand, the increase of framework aluminum leads to the imbalance of framework charge, resulting in more  $\text{Cu}^{2+}$  coordination with it, and at the same time, the Lewis acid caused by  $\text{Cu}^{2+}$  is also improved.

### 3.3.4. The effect of Ce addition on the reaction mechanism

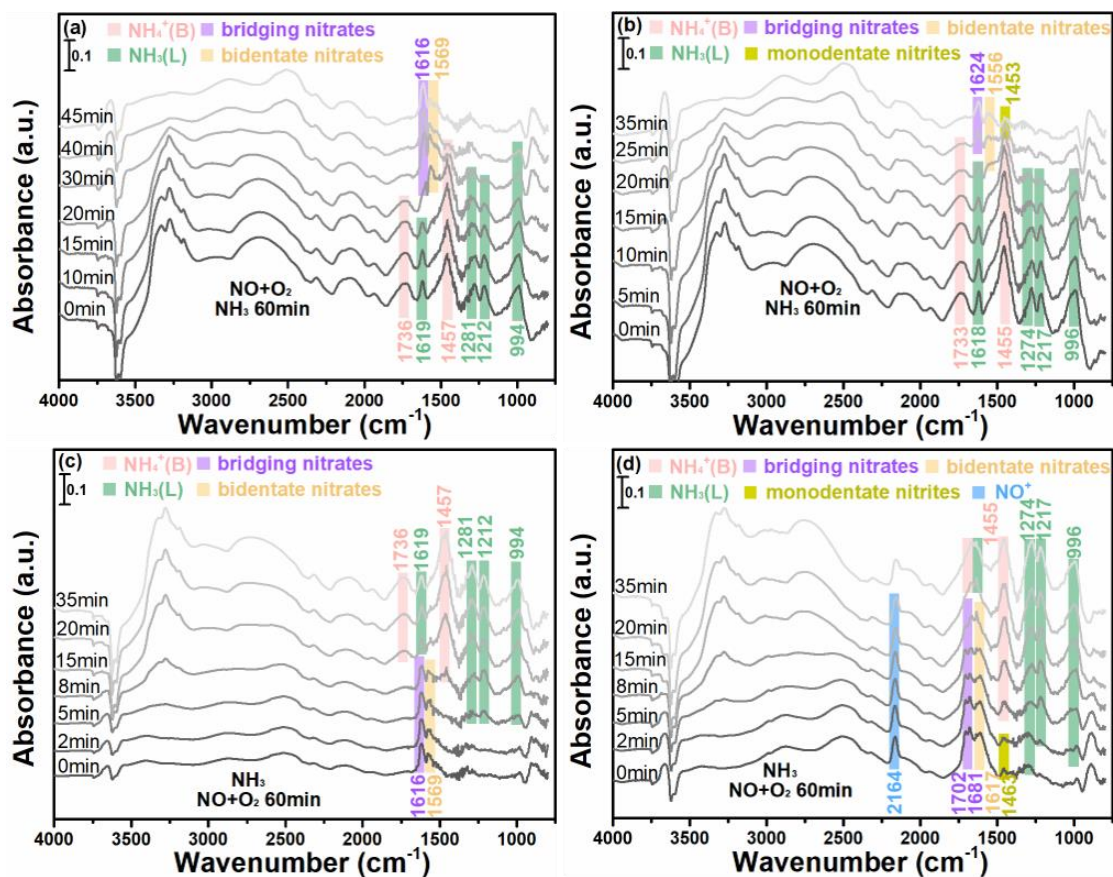


**Fig. 7.** In situ DRIFTS spectra of (a) Cu-SAPO-18 and (b) CuCe-SAPO-0.31 with pre-adsorbed  $\text{NH}_3$  species at  $150^\circ\text{C}$  during the reaction of  $\text{NO}+\text{O}_2$ . In situ DRIFTS spectra of (c) Cu-SAPO-18 and (d) CuCe-SAPO-0.31 with pre-adsorbed  $\text{NO}+\text{O}_2$  species at  $150^\circ\text{C}$  during the reaction of  $\text{NH}_3$ .

The formation and transformation of adsorbed species on the surface of Cu-SAPO-18 and CuCe-SAPO-x samples were studied by in situ DRIFTS experiments, and the effects of Ce addition on the activation capacity, reaction pathway of the intermediates and reaction mechanism were clarified.  $\text{NH}_3$  was used as the probe molecule to detect the surface acid sites of the catalyst (Fig. S13). The bands centered at 1619, 1281, 1212, and  $994\text{ cm}^{-1}$  were designated as the asymmetric and symmetric bending vibrations of the N-H bond, corresponding to the  $\text{NH}_3$  attached to the Lewis acid site [65–67]. The bands at 1736 and  $1457\text{ cm}^{-1}$  were owing to the symmetric and asymmetric bending

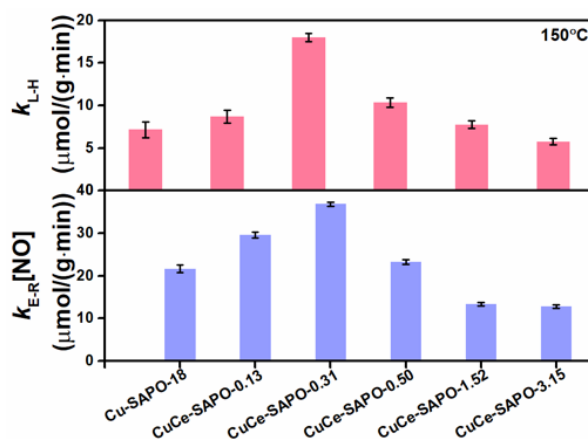
vibrations of the  $\text{NH}_4^+$  substance at the Brønsted acid site [65–67]. Comparing the peak strength of Fig. S13a, b, it can be seen that the acid strength on the surface of the catalyst increases after Ce addition, which is conducive to the adsorption and activation of ammonia, resulting in excellent  $\text{NH}_3$ -SCR activity over the entire temperature range. To illustrate the nitrate species formed during the reaction, we recorded the DRIFTS spectra of  $\text{NO}+\text{O}_2$  co-adsorption on Cu-SAPO-18 and CeCu-SAPO-0.31 samples at 150 °C, as shown in Fig. S14. The Cu-SAPO-18 catalyst mainly forms bridging nitrates ( $1616\text{ cm}^{-1}$ ) and bidentate nitrates ( $1569\text{ cm}^{-1}$ ). In addition to bridging nitrates and bidentate nitrates, monodentate nitrites ( $1463\text{ cm}^{-1}$ ) and  $\text{NO}^+$  species ( $2164\text{ cm}^{-1}$ ) were also formed over CuCe-SAPO-0.31 catalyst [65–67]. The  $\text{NO}^+$  species are mainly derived from the dimerization and disproportionation reactions of nitrogen dioxide. The addition of Ce changed the adsorption capacity of  $\text{NO}+\text{O}_2$  on Cu-SAPO-18 catalyst. The number of  $\text{NO}_x$  species adsorbed on CuCe-SAPO-0.31 catalyst increased, and the peak strength increased, indicating that the addition of Ce promoted the adsorption and activation of NO on the catalyst surface.

Fig. 7a showed the DRIFTS spectrum of the reaction between  $\text{NO}+\text{O}_2$  and preadsorbed  $\text{NH}_3$  on the Cu-SAPO-18 sample at 150 °C. When the sample surface was saturated with  $\text{NH}_3$ , absorption bands attributable to Lewis acid sites ( $1619, 1281, 1212,$  and  $994\text{ cm}^{-1}$ ) and Brønsted acid sites ( $1736$  and  $1457\text{ cm}^{-1}$ ) were detected. After the introduction of  $\text{NO}+\text{O}_2$ ,  $\text{NH}_3$  (L) species ( $1281, 1212, 1619,$  and  $994\text{ cm}^{-1}$ , decreasing from 8 min) were quickly consumed, but  $\text{NH}_4^+$  (B) species ( $1457\text{ cm}^{-1}$ ) were consumed slowly. The results showed that  $\text{NH}_3$  (L) acted as the main active intermediate and

reacted with NO in the gaseous phase, following Eley-Rideal (E-R) mechanism. After that, the excessive introduction of NO+O<sub>2</sub> resulted in the formation and accumulation of nitrate species on the sample surface, leading to the appearance of bridging nitrate (1616 cm<sup>-1</sup>) and bidentate nitrate (1567 cm<sup>-1</sup>). The CuCe-SAPO-0.31 catalyst also follows the E-R mechanism, similar to Cu-SAPO-18. Comparing Fig. 7a, b, the CuCe-SAPO-0.31 catalyst has a stronger NH<sub>3</sub> activation ability, and the NH<sub>3</sub> (L) species is consumed faster (decreasing from 3 minutes), which is considered to be the initial intermediates of the E-R mechanism. Because the partial substitution of Cu by Ce induced the coordinated unsaturated cation sites of the CeCu-SAPO-0.31 sample, more Lewis acid sites were formed [18]. The production of NH<sub>3</sub> (L) species is believed to increase low-temperature activity. Fig. 7c, d showed the DRIFTS spectrum of the reaction between the preadsorbed NO+O<sub>2</sub> and NH<sub>3</sub> on Cu-SAPO-18 and CuCe-SAPO-0.31 samples at 150 °C. For the Cu-SAPO-18 sample, the peak of nitrate species was gradually consumed after the introduction of NH<sub>3</sub>, and then the surface of the sample was mainly covered by adsorbed NH<sub>3</sub> species. It is proved that the reaction between NH<sub>3</sub> and adsorbed NO<sub>x</sub> species on Cu-SAPO-18 follows the Langmuir-Hinshelwood (L-H) mechanism. In the CuCe-SAPO-0.31 sample, the bridging (1702 cm<sup>-1</sup>), bidentate nitrate (1617 cm<sup>-1</sup>) and monodentate nitrite (1463 cm<sup>-1</sup>) formed after preadsorption of NO+O<sub>2</sub> was quickly consumed after introduced NH<sub>3</sub>, indicating that it also follows the L-H mechanism.

Through in situ DRIFTS results, it was found that both the L-H and E-R mechanisms on the Cu-SAPO-18 and CuCe-SAPO-0.31 catalysts occurred during the

NH<sub>3</sub>-SCR reaction. For the L-H mechanism, Ce doping increases the isolated Cu<sup>2+</sup> content, which is conducive to the adsorption and activation of NO molecules, especially the formation of NO<sup>+</sup>, which is transformed from the dimerization and disproportionation of nitrogen dioxide. Therefore, the "fast SCR" reaction promotes the reaction between the adsorbed NO+O<sub>2</sub> species and NH<sub>3</sub>, and further improves the low-temperature activity. For the E-R mechanism, the NH<sub>3</sub> (L) species is considered the most important initial intermediates. Due to the coordinated unsaturated cation sites induced by the introduction of Ce, more Lewis acid sites were generated in the CuCe-SAPO-0.31 sample, thus promoting the production of NH<sub>3</sub> (L) species. The kinetic test was further explained below.



**Fig. 8.** Rate constants of the SCR reaction following the Eley-Rideal mechanism ( $k_{E-R}$ ) and the Langmuir-Hinshelwood mechanism ( $k_{L-H}$ ).

The effect of cerium on the NH<sub>3</sub>-SCR reaction mechanism is studied following the early reports [68–70]. By linear regression shown in Fig. S15, the  $k_{L-H}$  and  $k_{E-R}$  representing the rate constant according to the Langmuir-Hinshelwood (L-H) and Eley-Rideal (E-R) mechanisms are obtained and depicted in Fig. 8 and Table S11. It is first found that loading with 0.13 and 0.31 wt.% of cerium promote both  $k_{L-H}$  and  $k_{E-R}$

constants, while more cerium leads to the reduction of the rate constants. This result is well coincided with the deNO<sub>x</sub> activity of fresh samples shown in Fig. S3a, which suggests that a small content of cerium increases the catalytic activity. In addition, the value of  $k_{E-R}[\text{NO}]$  is found greater than the  $k_{L-H}$ , suggesting that the E-R mechanism dominates the reaction process (Table S11). Next, although loading cerium has been confirmed to affect both  $k_{L-H}$  and  $k_{E-R}$ , notably, a small amount of Ce addition significantly increased  $k_{L-H}$ , indicating that Ce addition mainly affects the L-H mechanism.

#### 4. Conclusions

In conclusion, the one-pot synthesis method led to the introduction of cerium in the CuCe-SAPO-x catalysts with different cerium loading (0–3.15 wt.%). The use of the direct synthesis method and TEPA as a template allowed cerium species to be introduced in the ion-exchange sites of Cu-SAPO-18 in the form of Ce<sup>3+</sup> ions even with high loading (3.15 wt.%). The influence of cerium in the CuCe-SAPO-x catalysts on NH<sub>3</sub>-SCR performance was studied. The presence of cerium is found to improve the low-temperature activity (<200 °C) and hydrothermal stability of the catalyst. Adding a small amount of Ce affects the coordination of Si and Al atoms, resulting in more framework aluminum. Si(10Al) and Si(20Al) increase the Brønsted acid in the zeolite framework. At the same time, due to the imbalance of the skeleton charge, more Cu<sup>2+</sup> coordination is caused, which makes Lewis acid increase. This is conducive to improving the E-R and L-H mechanisms, which improves the low-temperature SCR property of the catalyst.

## **Declaration of Interests**

The authors declare that they have no known competing financial interests or personal relationships that could have appeared to influence the work reported in this paper.

## **Acknowledgments**

We thank the National Natural Science Foundation of China (21876093 and 52070114) for financial support.

## **References**

- [1] J. Kagawa, Health effects of diesel exhaust emissions-a mixture of air pollutants of worldwide concern, *Toxicol.* 181 (2002) 349–353.
- [2] Y. Ye, Z. Zang, T. Zhou, F. Dong, S. Lu, X. Tang, W. Wei, Y. Zhang, Theoretical and experimental investigation of highly photocatalytic performance of CuInZnS nanoporous structure for removing the NO gas, *J. Catal.* 357 (2018) 100–107.
- [3] M. Li, X. Liu, L. Wang, F. Hou, S. X. Dou, J. Liang, Rational design on photo(electro)catalysts for artificial nitrogen looping, *EcoMat.* 3 (2021) 12096–12121.
- [4] F. Liu, Y. Yu, H. He, Environmentally-benign catalysts for the selective catalytic reduction of NO<sub>x</sub> from diesel engines: structure-activity relationship and reaction mechanism aspects, *Chem. Commun.* 50 (2014) 8445–8463.
- [5] I. Nova, E. Tronconi, Urea-SCR technology for deNO<sub>x</sub> after treatment of diesel exhausts, *Johnson Matthey Technol. Rev.* 59 (2015) 221–232.
- [6] W. Shan, H. Song, Catalysts for the selective catalytic reduction of NO<sub>x</sub> with NH<sub>3</sub>

- at low temperature, *Catal. Sci. Technol.* 5 (2015) 4280–4288.
- [7] H. Chen, S. Mulla, E. Weigert, K. Camm, T. Ballinger, J. Cox, P. Blakeman, Cold start concept (CSC™): a novel catalyst for cold start emission control, *SAE Int. J. Fuels Lubr.* 6 (2013) 372–381.
- [8] Y. Gu, W. S. Epling, Passive NO<sub>x</sub> adsorber: an overview of catalyst performance and reaction chemistry, *Appl. Catal. A-Gen.* 570 (2019) 1–14.
- [9] J. Lee, J. R. Theis, E. A. Kyriakidou, Vehicle emissions trapping materials: successes, challenges, and the path forward, *Appl. Catal. B-Environ.* 243 (2019) 397–414.
- [10] S. Mohan, P. Dinesha, S. Kumar, NO<sub>x</sub> reduction behavior in copper zeolite catalysts for ammonia SCR systems: a review, *Chem. Eng. J.* 384 (2019) 1–10.
- [11] E. Borfecchia, P. Beato, S. Svelle, U. Olsbye, C. Lamberti, S. Bordiga, Cu-CHA - a model system for applied selective redox catalysis, *Chem. Soc. Rev.* 47 (2018) 8097–8133.
- [12] M. Moliner, C. Franch, E. Palomares, M. Grill, A. Corma, Cu-SSZ-39, an active and hydrothermally stable catalyst for the selective catalytic reduction of NO<sub>x</sub>, *Chem. Commun.* 48 (2012) 8264–8266.
- [13] J. Ma, Y. Li, J. Liu, Z. Zhao, C. Xu, Y. Wei, W. Song, Y. Sun, X. Zhang, Cu-SAPO-18 for NH<sub>3</sub>-SCR reaction: the effect of different aging temperatures on Cu<sup>2+</sup> active sites and catalytic performances, *Ind. Eng. Chem. Res.* 58 (2019) 2389–2395.
- [14] R. Martínez-Franco, M. Moliner, A. Corma, Direct synthesis design of Cu-SAPO-18, a very efficient catalyst for the SCR of NO<sub>x</sub>, *J. Catal.* 319 (2014) 36–43.

- [15] E. W. Mcfarland, H. Metiu, Catalysis by doped oxides, *Chem. Rev.* 113 (2012) 4391–4427.
- [16] C. Kuo, Y. Lu, P. Arab, K. S. Weeraratne, H. El-Kaderi, A. M. Karim, 18.1% single palladium atom catalysts on mesoporous covalent organic framework for gas phase hydrogenation of ethylene, *Cell Rep. Phy. Sci.* 2 (2021) 100495–100507.
- [17] X. Ji, T. Wang, Q. Liu, Y. Luo, S. Lu, G. Chen, S. Gao, A. M. Asiri, X. Sun, Oxidation-etching induced morphology regulation of Cu catalysts for high-performance electrochemical N<sub>2</sub> reduction, *EcoMat.* (2020) 1–7.
- [18] S. Han, J. Cheng, Q. Ye, S. Cheng, T. Kang, H. Dai, Ce doping to Cu-SAPO-18: enhanced catalytic performance for the NH<sub>3</sub>-SCR of NO in simulated diesel exhaust, *Micropor. Mesopor. Mat.* 276 (2019) 133–146.
- [19] Z. Chen, L. Guo, H. Qu, L. Liu, H. Xie, Q. Zhong, Controllable positions of Cu<sup>2+</sup> to enhance low-temperature SCR activity on novel Cu-Ce-La-SSZ-13 by a simple one-pot method, *Chem. Commun.* 56 (2020) 2360–2363.
- [20] B. Dou, G. Lv, C. Wang, Q. Hao, K. Hui, Cerium doped copper/ZSM-5 catalysts used for the selective catalytic reduction of nitrogen oxide with ammonia, *Chem. Eng. J.* 270 (2015) 549–556.
- [21] Y. Cao, Sha. Zou, L. Lam, Z. Yang, H. Xu, T. Lin, M. Gong, Y. Chen, Promotional effect of Ce on Cu-SAPO-34 monolith catalyst for selective catalytic reduction of NO<sub>x</sub> with ammonia, *J. Mol. Catal. A* 398 (2015) 304–311.
- [22] Z. Zhao, R. Yu, C. Shi, H. Gies, F. Xiao, D. D. Vos. T. Yokoi, X. Bao, U. Kolb, R. McGuire, A. N. Parvulescu, S. Manrer, U. Muller, W. Zhang, Rare-earth ion exchanged

Cu-SSZ-13 zeolite from organotemplate-free synthesis with enhanced hydrothermal stability in NH<sub>3</sub>-SCR of NO<sub>x</sub>, *Catal. Sci. Technol.* 9 (2019) 241–251.

[23] T. Usui, Z. Liu, S. Ibe, J. Zhu, C. Anand, H. Igarashi, N. Onaya, Y. Sasaki, Y. Shiramata, T. Kusmoto, T. Wakihara, Improve the hydrothermal stability of Cu-SSZ-13 zeolite catalyst by loading a small amount of Ce, *ACS Catal.* 8 (2018) 9165–9173.

[24] J. Fan, P. Ning, Y. Wang, Z. Song, X. Liu, H. Wang, J. Wang, L. Wang, Q. Zhang, Significant promoting effect of Ce or La on the hydrothermal stability of Cu-SAPO-34 catalyst for NH<sub>3</sub>-SCR reaction, *Chem. Eng. J.* 369 (2019) 908–919.

[25] Y. J. Kim, J. K. Lee, K. M. Min, B. S. Hong, I. S. Nam, B. K. Cho, Hydrothermal stability of Cu-SSZ-13 for reducing NO<sub>x</sub> by NH<sub>3</sub>, *J. Catal.* 311 (2014) 447–457.

[26] D. Wang, Y. Jangjou, Y. Liu, M. K. Sharma, J. Li, K. Kamasamudram, W. S. Epling, A comparison of hydrothermal aging effects on NH<sub>3</sub>-SCR of NO over Cu-SSZ-13 and Cu-SAPO-34 catalysts, *Appl. Catal. B-Environ.* 165 (2015) 438–445.

[27] T. Du, H. Qu, Q. Liu, W. Ma, Synthesis, activity and hydrophobicity of Fe-ZSM-5@silicalite-1 for NH<sub>3</sub>-SCR, *Chem. Eng. J.* 262 (2015) 1199–1207.

[28] T. Zhang, F. Qiu, J. Li, Design and synthesis of core-shell structured meso-Cu-SSZ-13@mesoporous aluminosilicate catalyst for SCR of NO with NH<sub>3</sub>: enhancement of activity, hydrothermal stability and propene poisoning resistance, *Appl. Catal. B-Environ.* 195 (2016) 48–58.

[29] Y. Li, W. Song, J. Liu, Z. Zhao, M. Gao, Y. Wei, Q. Wang, J. Deng, The protection of CeO<sub>2</sub> thin film on Cu-SAPO-18 catalyst for highly stable catalytic NH<sub>3</sub>-SCR performance, *Chem. Eng. J.* 330 (2017) 926–935.

- [30] K. Leistner, L. Olsson, Deactivation of Cu/SAPO-34 during low-temperature NH<sub>3</sub>-SCR, *Appl. Catal. B-Environ.* 165 (2015) 192–199.
- [31] J. Wang, D. Fan, T. Yu, J. Wang, T. Hao, X. Hu, M. Shen, W. Li, Improvement of low-temperature hydrothermal stability of Cu/SAPO-34 catalysts by Cu<sup>2+</sup> species, *J. Catal.* 322 (2015) 84–90.
- [32] S. Xiong, X. Xiao, Y. Liao, H. Dang, W. Shan, S. Yang, Global kinetic study of NO reduction by NH<sub>3</sub> over V<sub>2</sub>O<sub>5</sub>-WO<sub>3</sub>/TiO<sub>2</sub>: relationship between the SCR performance and the key factors, *Ind. Eng. Chem. Res.* 54 (2015) 11011–11023.
- [33] S. Yang, F. Qi, S. Xiong, H. Dang, Y. Liao, K. P. Wong, J. Li, MnO<sub>x</sub> supported on Fe-Ti spinel novel Mn based low temperature SCR catalyst with a high N<sub>2</sub> selectivity, *Appl. Catal. B-Environ.* 181 (2016) 570–580.
- [34] N. Usberti, M. Jablonska, M. D. Blasi, P. Forzatti, L. Lietti, A. Beretta, Design of a high-efficiency NH<sub>3</sub>-SCR reactor for stationary applications. A kinetic study of NH<sub>3</sub> oxidation and NH<sub>3</sub>-SCR over V-based catalysts, *Appl. Catal. B-Environ.* 179 (2015) 185–195.
- [35] G. Kresse, J. Furthmüller, Efficiency of ab-initio total energy calculations for metals and semiconductors using a plane-wave basis set, *Comput. Mater. Sci.* 6 (1996) 15–50.
- [36] G. Kresse, J. Furthmüller, Efficient iterative schemes for ab initio total-energy calculations using a plane-wave basis set, *Phys. Rev. B* 54 (1996) 11169–11186.
- [37] M. Ernzerhof, K. Burke, M. Ernzerhof, Generalized gradient approximation made simple, *Phys. Rev. Lett.* 77 (1996) 3865–3868.

- [38] G. Kresse, D. Joubert, From ultrasoft pseudopotentials to the projector augmented-wave method, *Phys. Rev. B* 59 (1999) 1758–1775.
- [39] P. E. Blöchl, Projector augmented-wave method, *Phys. Rev. B* 50 (1994) 17953–17979.
- [40] S. L. Dudarev, G. A. Botton, S. Y. Savrasov, C. J. Humphreys, A. P. Sutton, Electron-energy-loss spectra and the structural stability of nickel oxide: an LSDA+U study, *Phys. Rev. B* 57 (1998) 1505–1510.
- [41] G. Henkelman, A. Arnaldsson, H. Jónsson, A fast and robust algorithm for bader decomposition of charge density, *Comput. Mater. Sci.* 36 (2006) 354.
- [42] Z. Chen, C. Fan, L. Pang, S. Ming, W. Guo, P. Liu, H. Chen, T. Li, One-pot synthesis of high performance Cu-SAPO-18 catalyst for NO reduction by NH<sub>3</sub>-SCR: influence of silicon content on the catalytic properties of Cu-SAPO-18, *Chem. Eng. J.* 348 (2018) 608–617.
- [43] M. Aziza, A. F. Ismail, X-Ray photoelectron spectroscopy (XPS), *Mem. Chara.* 5 (2017) 81–93.
- [44] A. M. Venezia, X-ray photoelectron spectroscopy (XPS) for catalysts characterization, *Catal. Today* 77 (2003) 359–370.
- [45] L. Yuliati, T. Hamajima, T. Hattori, H. Yoshida, Highly dispersed Ce(III) species on silica and alumina as new photocatalysts for non-oxidative direct methane coupling, *Chem. Commun.* 10 (2005) 4824–4826.
- [46] C. Fan, Z. Chen, L. Pang, S. Ming, X. Zhang, K. B. Albert, P. Liu, H. P. Chen, T. Li, The influence of Si/Al ratio on the catalytic property and hydrothermal stability of

- Cu-SSZ-13 catalysts for NH<sub>3</sub>-SCR, *Appl. Catal. A-Gen.* 550 (2018) 256–265.
- [47] S. Han, Q. Ye, S. Cheng, T. Kang, H. Dai, Effect of the hydrothermal aging temperature and Cu/Al ratio on the hydrothermal stability of CuSSZ-13 catalysts for NH<sub>3</sub>-SCR, *Catal. Sci. Technol.* 703 (2017) 703–717.
- [48] L. Ma, Y. Cheng, G. Cavataio, R. W. McCabe, L. Fu, J. Li, Characterization of commercial Cu-SSZ-13 and Cu-SAPO-34 catalysts with hydrothermal treatment for NH<sub>3</sub>-SCR of NO<sub>x</sub> in diesel exhaust, *Chem. Eng. J.* 225 (2013) 323–330.
- [49] Y. Li, J. Deng, W. Song, J. Liu, Z. Zhao, M. Gao, Y. Wei, L. Zhao, Nature of Cu species in Cu-SAPO-18 catalyst for NH<sub>3</sub>-SCR: combination of experiments and DFT calculations, *J. Phys. Chem. C* 120 (2016) 14669–14680.
- [50] V. Mohan, B. Dutta, R. Ripani, P. K. Jain, Room-temperature catalyst-free methane chlorination, *Cell Rep. Phy. Sci.* 2 (2021) 100545–100554.
- [51] J. Song, Y. Wang, E. D. Walter, N. M. Washton, D. Mei, L. Kovarik, M. H. Engelhard, S. Prodinger, Y. Wang, C. H. F. Peden, F. Gao, Toward rational design of Cu/SSZ-13 selective catalytic reduction catalysts: implications from atomic-level understanding of hydrothermal stability, *ACS Catal.* 7 (2017) 8214–8227.
- [52] H. Jiang, B. Guan, X. Peng, R. Zhan, H. Lin, Z. Huang, Influence of synthesis method on catalytic properties and hydrothermal stability of Cu/SSZ-13 for NH<sub>3</sub>-SCR reaction, *Chem. Eng. J.* 379 (2020) 122358–122373.
- [53] K. J. Hun, H. Zhu, J. H. Lee, C. H. F. Peden, J. Szanyi, Two different cationic positions in Cu-SSZ-13? *Chem. Commun.* 48 (2012) 4476–4758.
- [54] F. Gao, Y. Wang, N. M. Washton, M. Kollar, J. Szanyi, C. H. F. Peden, Effects of

- alkali and alkaline earth cocations on the activity and hydrothermal stability of Cu/SSZ-13 NH<sub>3</sub>-SCR catalysts, *ACS Catal.* 5 (2015) 6780–6791.
- [55] J. Luo, F. Gao, K. Kamasamudram, N. Currier, C. H. F. Peden, A. Yezerets, New insights into Cu/SSZ-13 SCR catalyst acidity. Part I: Nature of acidic sites probed by NH<sub>3</sub> titration, *J. Catal.* 348 (2017) 291–299.
- [56] J. Yasser, Q. Do, Y. Gu, L. G. Lim, H. Sun, D. Wang, A. Kumar, J. Li, L. C. Grabow, W. S. Epling, Nature of Cu active centers in Cu-SSZ-13 and their responses to SO<sub>2</sub> exposure, *ACS Catal.* 8 (2018) 1325–1337.
- [57] A. Wang, P. Arora, D. Bernin, A. Kumar, K. Kamasamudram, Investigation of the robust hydrothermal stability of Cu/LTA for NH<sub>3</sub>-SCR reaction, *Appl. Catal. B-Environ.* 246 (2019) 242–253.
- [58] R. Xu, Z. Wang, N. Liu, C. Dai, J. Zhang, B. Chen, Understanding Zn functions on hydrothermal stability in a one-pot-synthesized Cu&Zn-SSZ-13 catalyst for NH<sub>3</sub> selective catalytic reduction, *ACS Catal.* 10 (2020) 6197–6212.
- [59] S. Ming, Z. Chen, C. Fan, L. Pang, W. Guo, K. B. Albert, P. Liu, T. Li, The effect of copper loading and silicon content on catalytic activity and hydrothermal stability of Cu-SAPO-18 catalyst for NH<sub>3</sub>-SCR, *Appl. Catal. A-Gen.* 559 (2018) 47–56.
- [60] T. Yu, D. Fan, T. Hao, J. Wang, M. Shen, W. Li, The effect of various templates on the NH<sub>3</sub>-SCR activities over Cu/SAPO-34 catalysts. The effect of various templates on the NH<sub>3</sub>-SCR activities over Cu/SAPO-34 catalysts, *Chem. Eng. J.* 243 (2014) 159–168.
- [61] T. Yu, J. Wang, M. Shen, W. Li, NH<sub>3</sub>-SCR over Cu/SAPO-34 catalysts with various

- acid contents and low Cu loading, *Catal. Sci. Technol.* 3 (2013) 3234–3245.
- [62] J. Wang, T. Yu, X. Wang, G. Qi, J. Xue, M. Shen, W. Li, The influence of silicon on the catalytic properties of Cu/SAPO-34 for NO<sub>x</sub> reduction by ammonia-SCR, *Appl. Catal. B-Environ.* 127 (2012) 137–147.
- [63] H. Zhao, X. Chen, A. Bhat, Y. Li, J.W. Schwank, Insight into hydrothermal aging effect on deactivation of Pd/SSZ-13 as low-temperature NO adsorption catalyst: Effect of dealumination and Pd mobility, *Appl. Catal. B-Environ.* 286 (2021) 119874–119887.
- [64] J. Zhang, Y. Shan, L. Zhang, J. Du, H. He, S. Han, C. Lei, S. Wang, W. Fan, Z. Feng, X. Liu, X. Meng, F.-S. Xiao, Importance of controllable Al sites in CHA framework by crystallization pathways for NH<sub>3</sub>-SCR reaction, *Appl. Catal. B-Environ.* 277 (2020) 119193–119201.
- [65] D. Wang, L. Zhang, K. Kamasamudram, W. S. Epling, In situ-DRIFTS study of selective catalytic reduction of NO<sub>x</sub> by NH<sub>3</sub> over Cu-exchanged SAPO-34, *ACS Catal.* 3 (2013) 871–881.
- [66] L. Ma, Y. S. Cheng, G. Cavataio, R. W. McCabe, L. X. Fu, J. H. Li, In situ DRIFTS and temperature-programmed technology study on NH<sub>3</sub>-SCR of NO<sub>x</sub> over Cu-SSZ-13 and Cu-SAPO-34 catalysts, *Appl. Catal. B-Environ.* 156 (2014) 428–437.
- [67] M. P. Ruggeri, I. Nova, E. Tronconi, J. A. Pihl, T. J. Toops, W. P. Partridge, In-situ DRIFTS measurements for the mechanistic study of NO oxidation over a commercial Cu-CHA catalyst, *Appl. Catal. B-Environ.* 166 (2015) 181–192.
- [68] S. Xiong, J. Weng, Y. Liao, Z. Li, Y. Geng, X. Xiao, N. Huang, S. Yang, Alkali metal deactivation on the low temperature selective catalytic reduction of NO<sub>x</sub> with

NH<sub>3</sub> over MnO<sub>x</sub>-CeO<sub>2</sub>: a mechanism study, *J. Phys. Chem. C* 120 (2016) 15299–15309.

[69] T. Yan, Q. Liu, S. Wang, G. Xu, M. Wu, J. Chen, J. Li, Promoter rather than inhibitor: phosphorus incorporation accelerates the activity of V<sub>2</sub>O<sub>5</sub>-WO<sub>3</sub>/TiO<sub>2</sub> catalyst for selective catalytic reduction of NO<sub>x</sub> by NH<sub>3</sub>, *ACS Catal.* 10 (2020) 2747–2753.

[70] S. Xiong, Y. Liao, X. Xiao, H. Dang, S. Yang, Novel effect of H<sub>2</sub>O on the low temperature selective catalytic reduction of NO with NH<sub>3</sub> over MnO<sub>x</sub>-CeO<sub>2</sub>: mechanism and kinetic study, *J. Phys. Chem. C* 119 (2015) 4180–4187.